Electronic Supplementary Material (ESI) for Physical Chemistry Chemical Physics.

SUPPORTING INFORMATION FOR

An Oxygen-Passivated Vanadium Cluster $[V@V_{10}O_{15}]1^-$ with Metal-Metal Coordination Produced by Reacting V_n^- with O_2

Hanyu Zhang,[†a] Chaonan Cui,[†a] Miao Yan,[†b] Lijun Geng,[a] Haiming Wu,[a] Yuhan Jia,[a] Zhixun Luo,[*a] and Si-Dian Li[*b]

[a] Beijing National Laboratory of Molecular sciences (BNLMS), State Key Laboratory for Structural Chemistry of Unstable and Stable Species, Institute of Chemistry, Chinese Academy of Sciences, Beijing 100190, China.

University of Chinese Academy of Sciences, Beijing 100049, China.

[b] Institute of Molecular Science, Shanxi University, Taiyuan 030006, China.

ξ These authors contributed equally to this work.

Contents

S1. Experimental and Theoretical Methods

1.1. Experimental methods

A customized reflection time-of-flight mass spectrometer (Re-TOFMS), coupled with a pulsed laser vaporization cluster source and an after-grow reaction tube, was utilized to study the formation and stability of anionic vanadium oxides.[1-4] The apparatus has been successfully applied in the research of the reactivity of vanadium (V_n^+) clusters[2] and aluminum (Al_n^+) clusters[3] towards oxygen and also the discovery of stable metal-benzene clusters[4], so a brief description is given here. The anionic vanadium clusters V_n^- were generated via a 30-mm long nozzle by laser ablation of a vanadium disk (99.9%) with a Nd:YAG (532 nm) laser. The buffer gas He (99.999%) was controlled by a pulsed general valve (Parker, Series 9) with a backing pressure of 1.0 MPa. After cluster generation, the V_n^- clusters reacted with diluted oxygen in the reaction tube to produce anionic vanadium oxides, and then the molecular beam was skimmed into the vacuum system of Re-TOFMS for mass abundance analysis. The reaction gas consisting of oxygen at concentrations of 5%, 10%, or 20% in helium at a pressure of 0.1 MPa was injected into the reaction tube by another pulsed general valve with an on time of 195 μs for each 100 ms period. The molecular number density of oxygen in the reaction tube for each concentration of reaction gas is estimated to be ~1.8×10^{19}, ~3.7×10^{19}, and ~7.4×10^{19} molecules/m^3, respectively.

1.2. Theoretical methods

Unbiased global-minimum searches were performed on $V_{11}O_{15}^-$ using both the ab initio evolutionary algorithm USPEX (Universal Structure Predictor: Evolutionary Xtallography)[5, 6] and the basin-hoping global minimum search using the TGMin code[7] at PBE (Perdew, Burke, and Ernzerhof) level[8]. More than 2200 structures were probed until the global minimum (GM) is found.

1.2.1 USPEX structural research and gaussian optimization

The stable structures of neutral V_nO_m clusters, including $V_{11}O_{15}$, $V_{11}O_{14}$, $V_{10}O_{14}$ and $V_{13}O_{17}$, are determined by a global search method using the ab initio evolutionary algorithm USPEX (Universal Structure Predictor: Evolutionary Xtallography), which has been successfully used to predict various crystal structures, nanoclusters and surfaces[5]. The first-generation structures were created using a randomly-selected symmetric point group, and the subsequent generations were produced by different variation operators, including heredity, soft mutation, permutation, and random symmetric generator. The structure maintaining the lowest enthalpy in 30 successive generations was considered as the most stable structure. During the global minimum optimization, all structures were relaxed using Vienna ab initio Simulation Package (VASP) software[6]. The PBE (Perdew, Burke, and Ernzerhof) functional and projector augmented wave (PAW) pseudopotentials were employed to describe the exchange and correlation potentials and the nuclei-electron interactions[8, 9]. The kinetic energy cutoff of the plane wave basis was set to 400 eV. All atoms were allowed to relax until the ionic relaxation reached the

convergence criteria of 0.02 eV/Å. More than 1200 structures have been calculated until the global minimum is found.

Low-lying structures were then fully optimized at the density functional theory (DFT) level of BP86,[10, 11] with the basis set of def2-TZVP,[12] implemented in the Gaussian 09 software package.[13] Details of the global-minimum searches are given in Fig. S7-S8 and Table S1 in ESI. All the DFT calculations were performed using tight convergence criteria and ultrafine level of integral lattice. The computational method (BP86/def2-TZVP) has been proved to provide accurate geometries for transition metal oxides and sulphides,[2, 14] and the test calculations utilizing this method provided consistent results (Table S1, ESI). Zero-point correction energies were used in this study.

1.2.2 TGMin structural research

To more conclusively determine the structure of $V_{11}O_{15}^-$, we have also conducted basin-hoping global minimum search using the TGMin code method,[7] which is based on a self-developed program used for global minimum searching for geometric structures, implemented with constrained basin-hopping (BH) algorithm. more than 1000 stationary points had been probed on the potential energy surface. As results, the global minimum structure of $V_{11}O_{15}^-$ (D_{5h}-geometry) is identical to that found by the aforementioned method.

1.2.3 Molecular dynamics simulations

Having determined the structure of $V_{11}O_{15}^-$ (D_{5h} geometry), Born–Oppenheimer molecular dynamics (BOMD) simulations were performed at 300 K, 600 K, 800 K, 1000 K, and 1200 K for 30 ps using the software suite of CP2K[15].

1.2.4 AdNDP and aromaticity analysis

The density matrix in the basis of the natural atomic orbitals (NAO) as well as the transformation between atomic orbital and natural atomic orbital basis sets was generated at the BP86/def2-TZVP level of theory by means of the NBO code[16] incorporated in Gaussian 09 software package. Bonding analyses were performed using the adaptive natural density partitioning (AdNDP)[17, 18] method which recovers both the localized and delocalized bonding elements of the concerned systems. The through space NMR shielding which was visualized as iso-chemical-shielding surfaces (ICSSs)[19, 20] is calculated on the basis of gauge-invariant atomic orbitals (GIAO)[21, 22] method. All the electronic wavefunction analyses were conducted by Multiwfn 3.7 software package[23] and VMD[24] was the visualization program for the structures and orbitals.

S2. Experimental Details

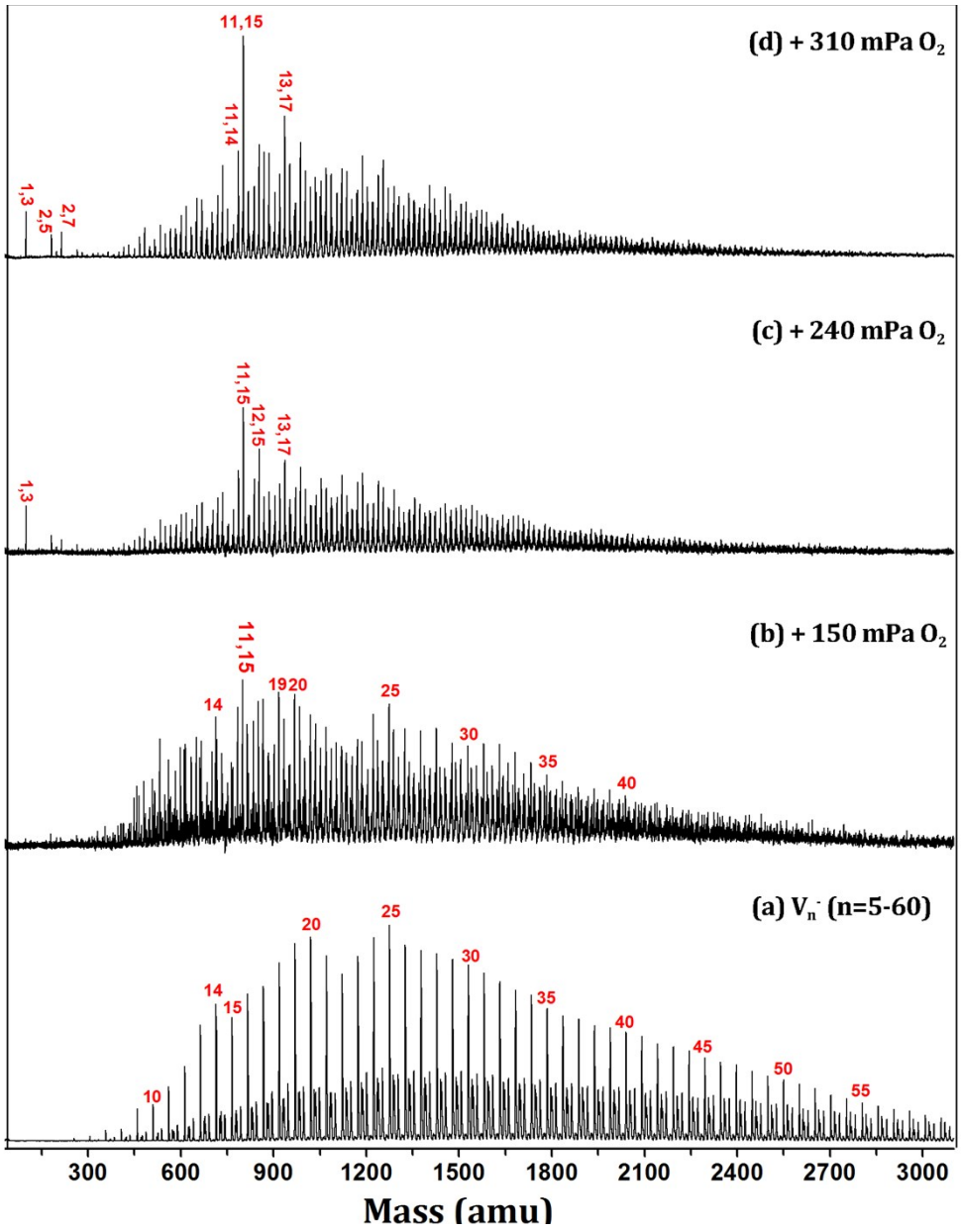

Fig. S1 The mass spectra of V_n^- , n=5-60 **(a)** and V_n^- reacting with different amounts of O_2 by 5%, 10%, and 20% O_2/He, respectively **(b-d)**.

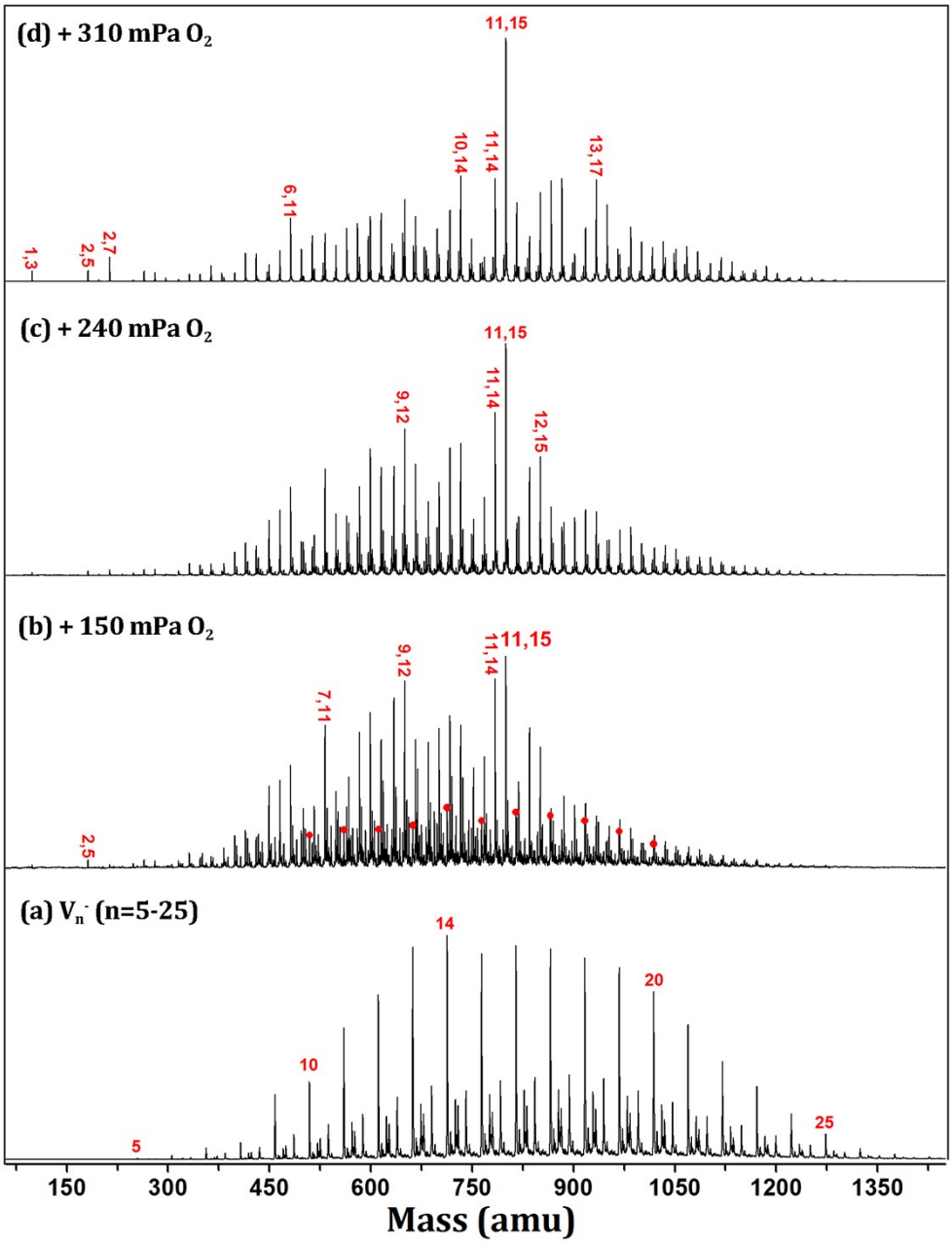

Fig. S2 The mass spectra of V_n^- , n=5-25 **(a)** and V_n^- reacting with different amounts of O_2 by 5%, 10%, and 20% O_2/He, respectively **(b-d)**.

S3 Calculation Details

3.1 Structural determination

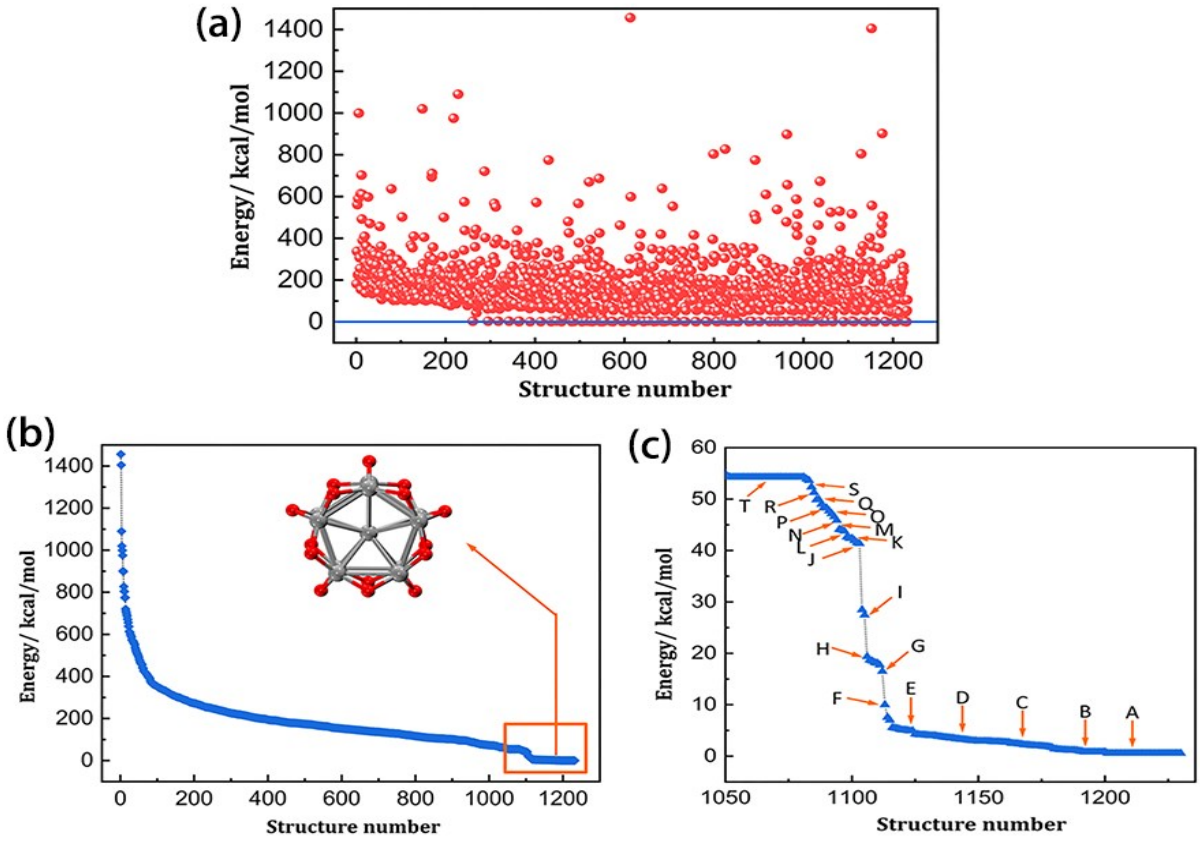

Fig. S3 (a) Progress of an evolutionary simulation for neutral $V_{11}O_{15}$ based on USPEX combined with VASP. The blue line shows the lowest energy structure and all the energies are relative to the global minimum structure. The evolutionary simulation used 20 structures per generation. Besides, the lowest-energy structure of the previous generation survived into the next generation. **(b)** presents the structures from high energy to low energy. **(c)** shows the structures with relative lower energies and the structures are labelled by arrows.

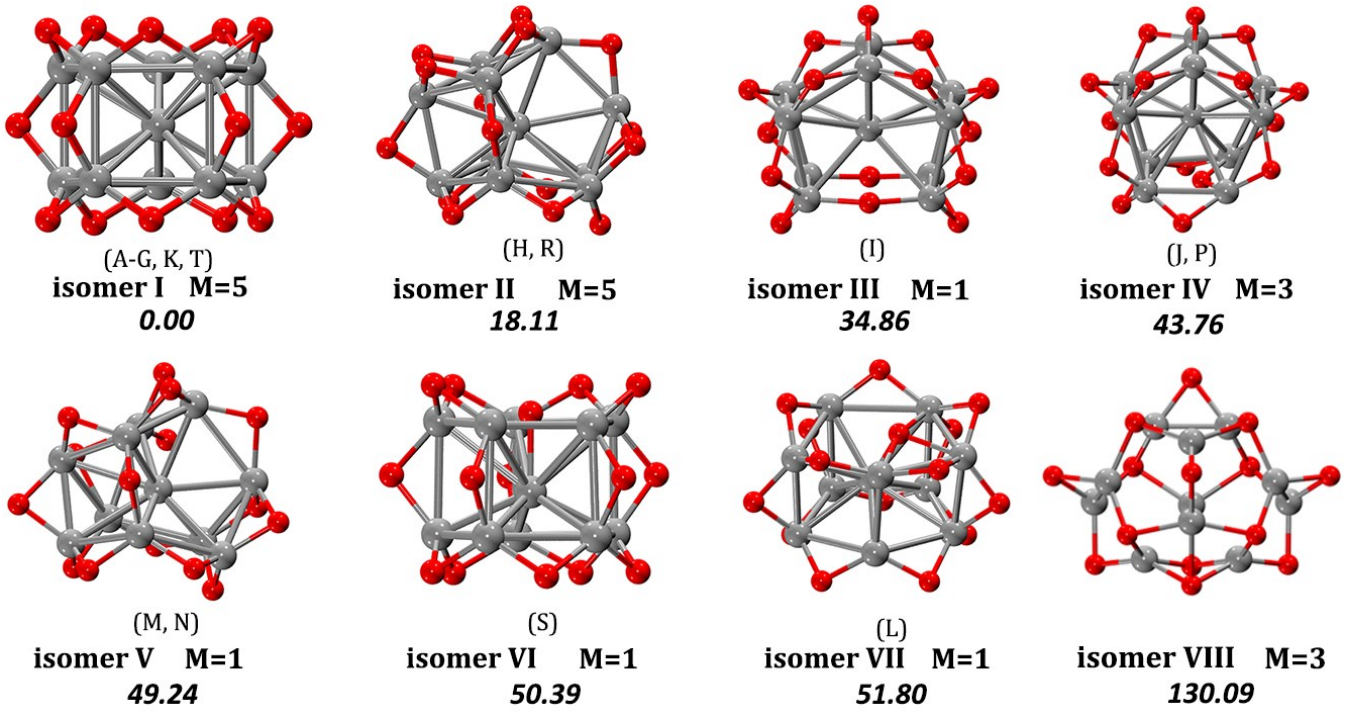

Fig. S4 The isomers of anionic $V_{11}O_{15}^-$ and their energy difference (ΔE_{ZPV}, kcal/mol) calculated at BP86/def2-TZVP level of theory. M indicates spin multiplicities. The initial geometric structures of these isomers are chosen from Fig.S6(c) and the corresponding characters are labelled in parentheses.

Table S1 A comparison of zero-vibration corrected energy differences (ΔE_{zpv}, kcal/mol) between different spin multiplicities of $V_{11}O_{15}^-$ calculated at different levels of theory.

	BP86/def2-TZVP	**BP86/TZVP[12]**	**BPw91(ref.[9, 11])/TZVP**	**B3LYP[11, 25, 26]/TZVP**
M=1	4.32	\	\	\
M=3	3.35	1.39	1.56	5.78
M=5	0.00	0.00	0.00	0.00
M=7	11.65	10.77	\	\

3.2 $V_{11}O_{15}^-$ fragmentation analysis

Table S2 The reaction energies for "$V_{13}^- + 10O_2 \rightarrow V_{11}O_{15}^- + V_2O_5$" calculated at different level of theory.

	BP86/def2-TZVP	BP86/def2-TZVPD	BPw91/TZVP	B3LYP/TZVP
ΔE (a.u.)	-3.217	-3.223	-2.381	-3.317

Table S3 Vertical ionization energy (VDE), O- and V- atom removal energies of $V_{11}O_{15}^-$ calculated at BP86/def2-TZVP level of theory.

Dissociation channel	ΔE
$V_{11}O_{15}^- \rightarrow V_{11}O_{15} + e^-$	3.66 eV
$V_{11}O_{15}^- \rightarrow V_{11}O_{14}^-(a) + O$	191.50 kcal/mol
$V_{11}O_{15}^- \rightarrow V_{11}O_{14}^-(b) + O$	192.07 kcal/mol
$V_{11}O_{15}^- \rightarrow V_{10}O_{15}^- + V$	239.74 kcal/mol
$V_{11}O_{15}^- \rightarrow V_{10}O_{14}^-(a) + VO$	137.98 kcal/mol
$V_{11}O_{15}^- \rightarrow V_{10}O_{14}^-(b) + VO$	146.02 kcal/mol

Note: The optimized structures are given in Fig. S5.

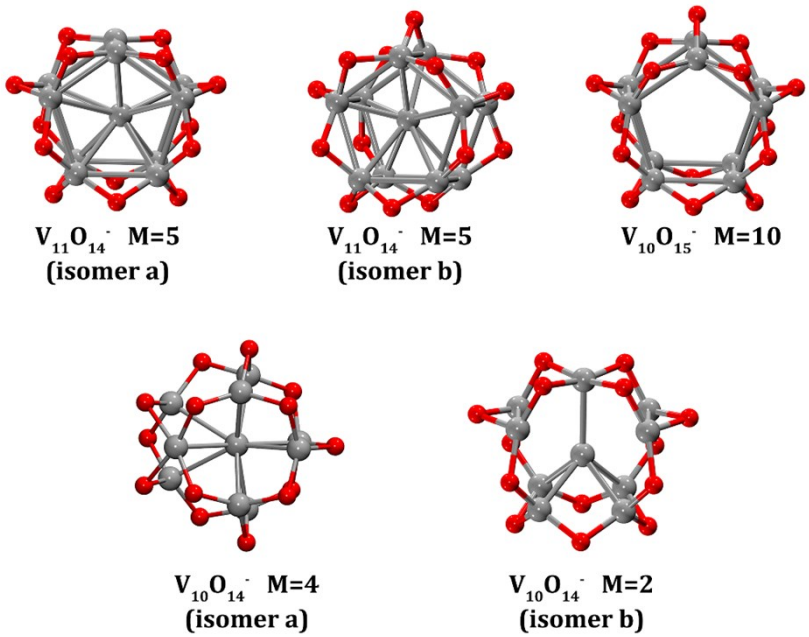

Fig. S5 The optimized structures of likely fragments that referred in Table S3 (M=spin multiplicities).

3.3 Stability and molecular dynamics simulation

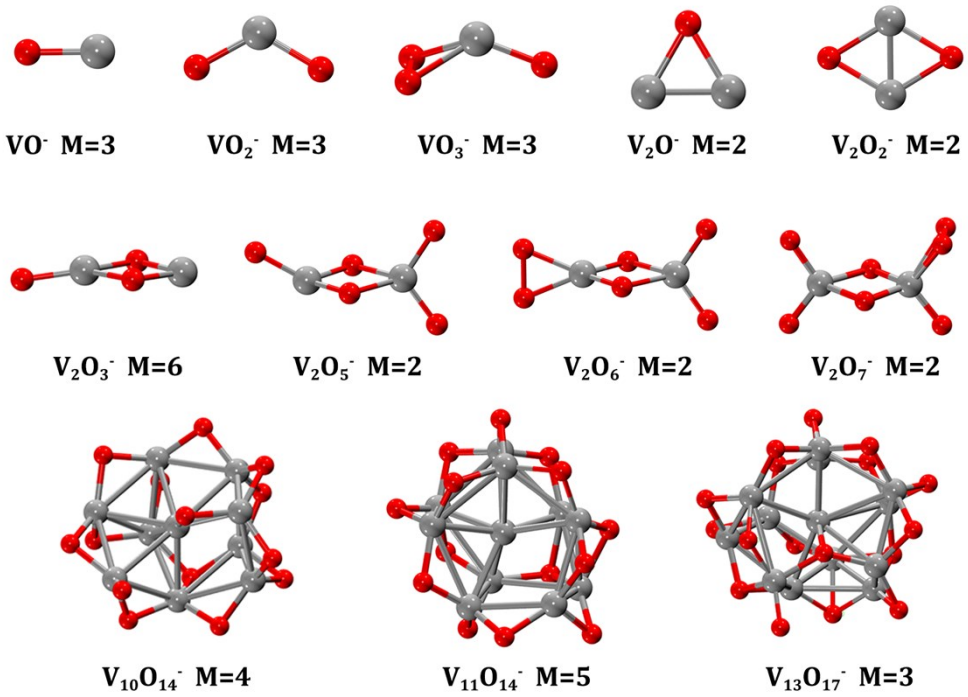

Fig. S6 The optimized structures of $V_nO_m^-$ clusters. The initial structures of $V_{10}O_{14}^-$, $V_{11}O_{14}^-$ and $V_{13}O_{17}^-$ (corresponding to Fig. 2a) are obtained by USPEX global research and optimized at BP86/def2-TZVP level, and the initial structures of other $V_nO_m^-$ clusters refer to the previous reported isomers which are proved to be relatively stable.[27-30] M indicates spin multiplicities.

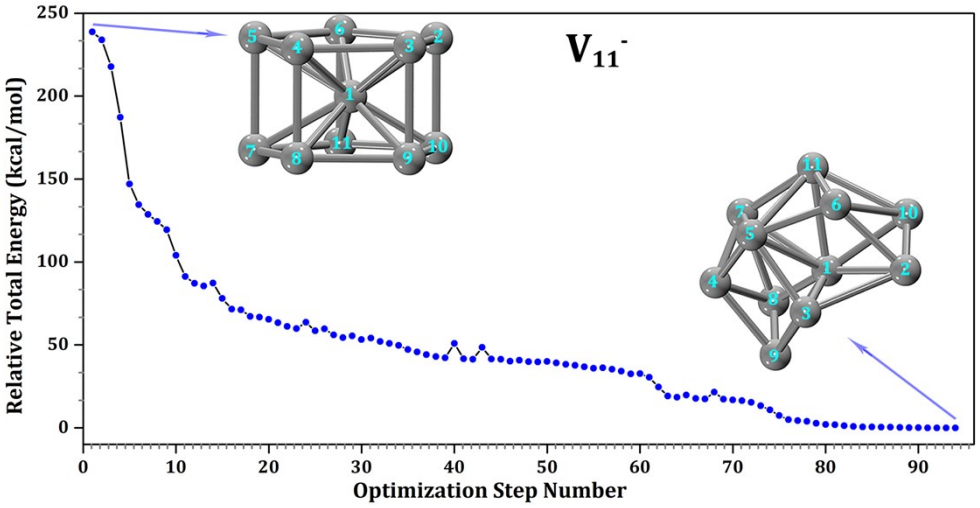

Fig. S7 Structural relaxation of naked V_{11}^- based on DFT calculations at BP86/def2-TZVP level of theory. The initial structure is the metal core of $V_{11}O_{15}^-$.

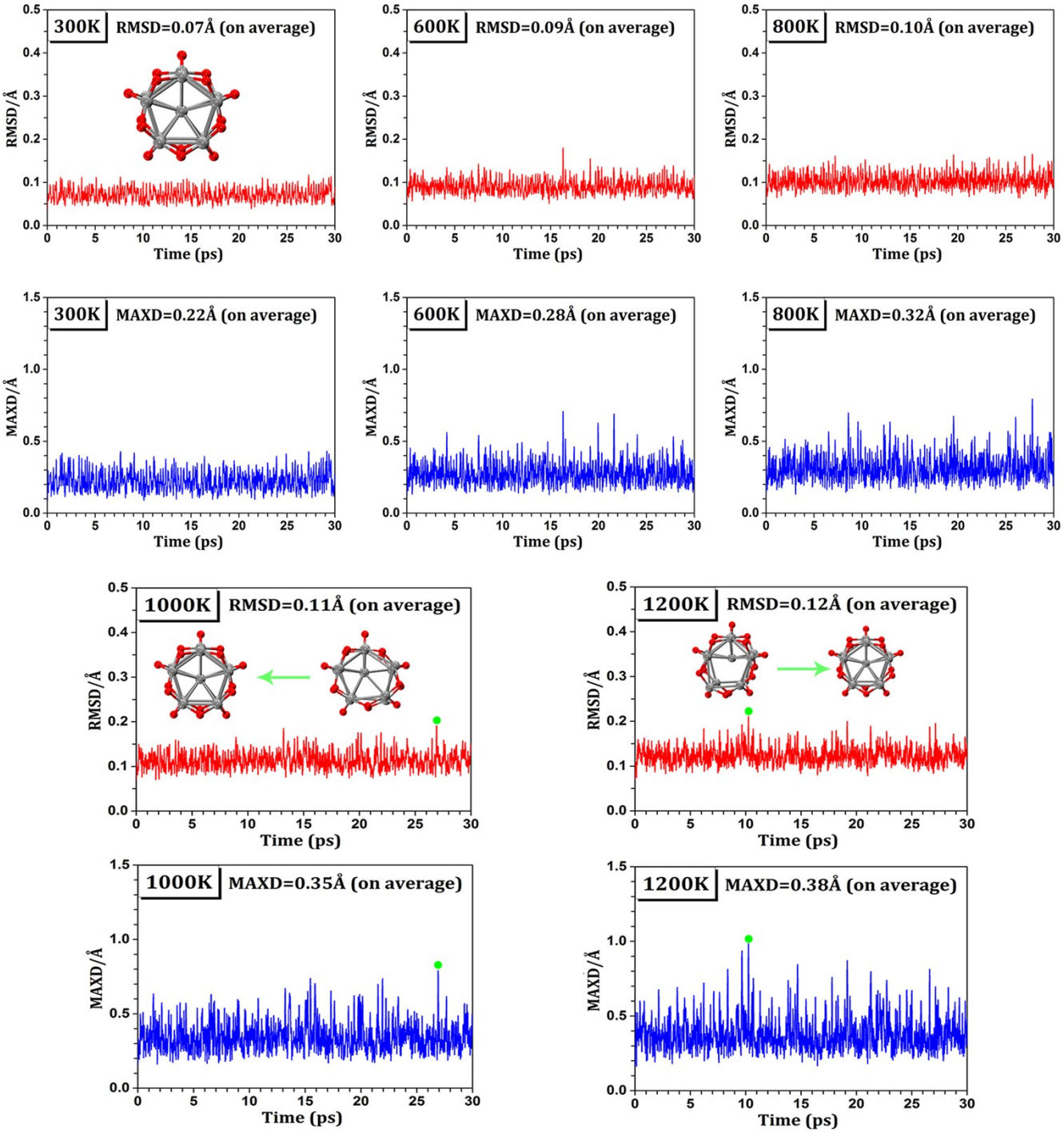

Fig. S8 Born-Oppenheimer molecular dynamics simulations of D_{5h} $V_{11}O_{15}^-$ at 300K, 600K, 800K, 1000K and 1200K for 30 ps, with the average root-mean-square-deviation (RMSD) values and maximum bond length deviation (MAXD) values indicated in Å.

3.4 Spin density

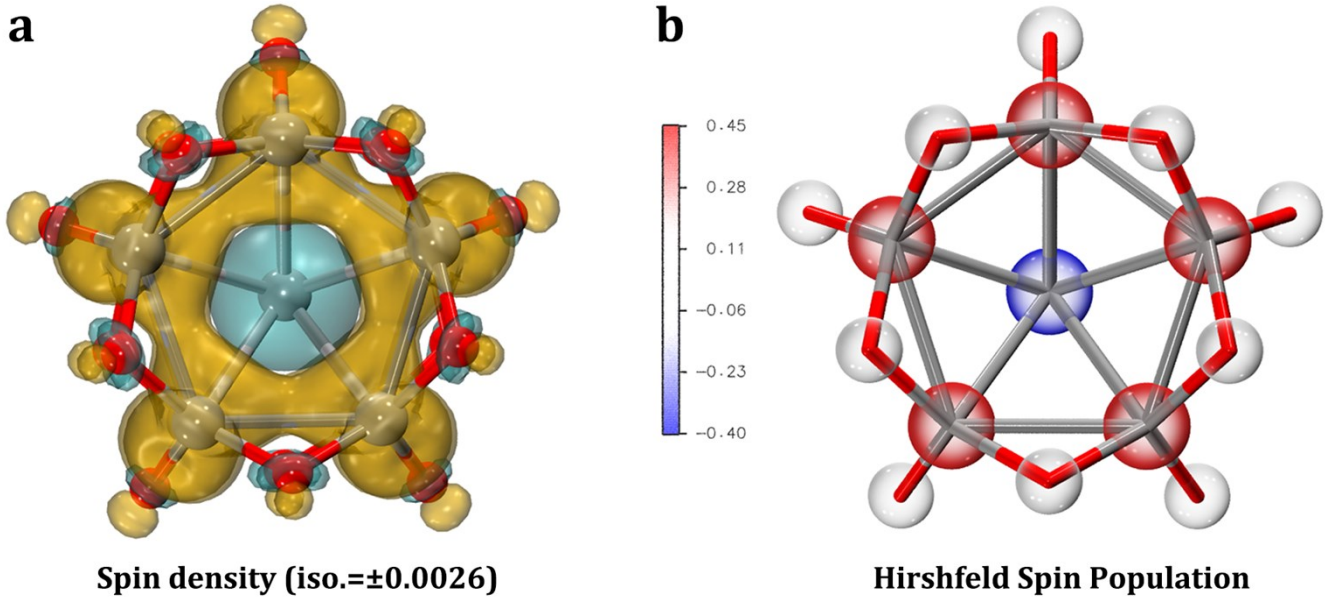

Fig. S9 (a) Spin density pattern of the $V_{11}O_{15}^-$. **(b)** Hirshfeld spin population of $V_{11}O_{15}^-$.

3.5 Electrostatic potential

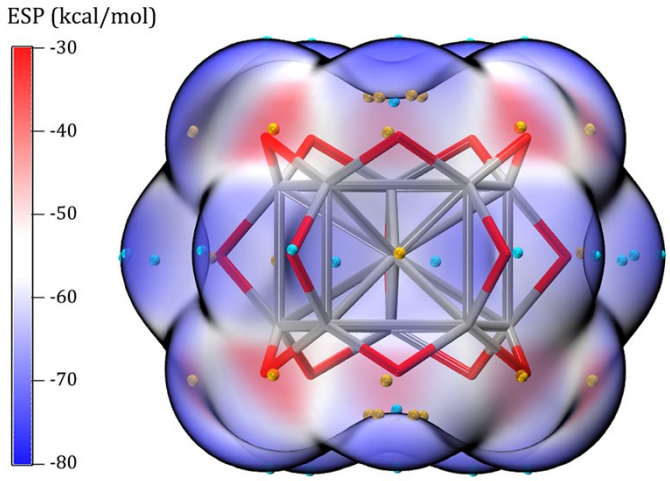

Fig. S10 Surface electrostatic potential (ESP) analysis of $V_{11}O_{15}^-$. The cyan dots indicate the minima of the surface electrostatic potential and the orange dots indicate the maxima of ESP.

Generally, the space indicated by vanadium atoms contains the maxima of electrostatic potential (ESP) and the minima of ESP locate in the space indicated by oxygen atoms. The enhanced stability of oxygen-bridge passivation of metal clusters is reminiscent of the M-S-M bonding in various thiol-protected metal clusters synthesized via wet chemistry.[31-38]

3.6 V_n^- clusters and energetics

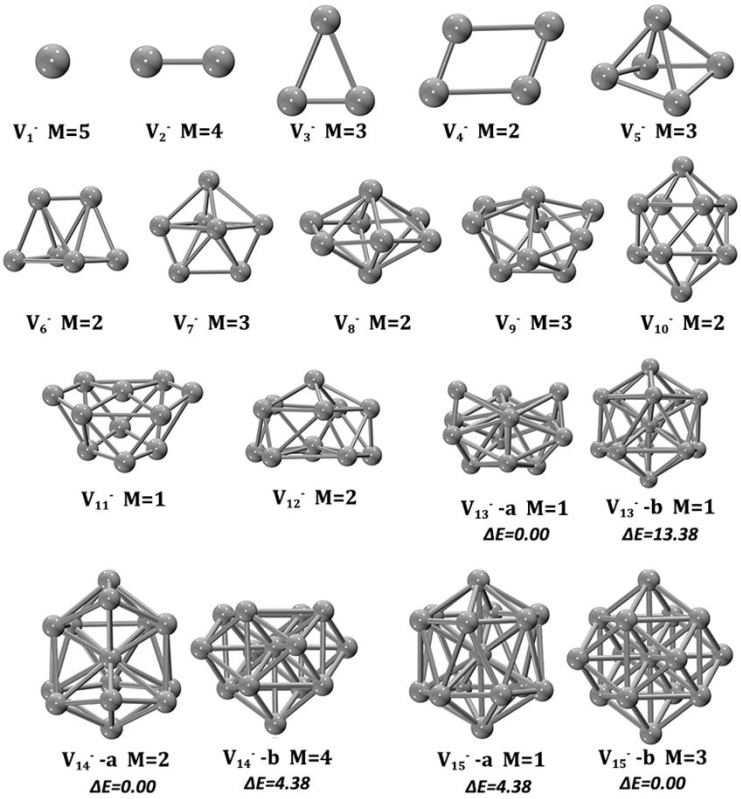

Fig. S11 The optimized structures of anionic V_n^- (n=1-15) at BP86/def2-TZVP level. M indicates spin multiplicities. Relative zero-point vibration corrected energies (ΔE_{ZPV}) between different isomers, given in kcal/mol.

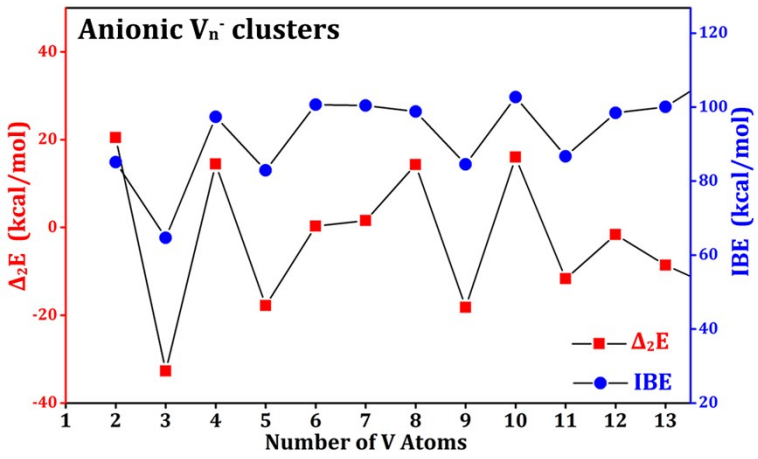

Fig. S12 Calculated incremental binding energies (blue ●) and the second-energy differences (red■) of the V_n^- clusters. Energies are given in kcal/mol. The binding energies and second-order binding energies of s are calculated according to the equations $IBE = E(V^0) + E(V_{n-1}^-) - E(V_n^-)$; $\Delta_2 E(n) = E(V_{n-1}^-) + E(V_{n+1}^-) - 2E(V_n^-)$.

3.7 Orbitals and density of states

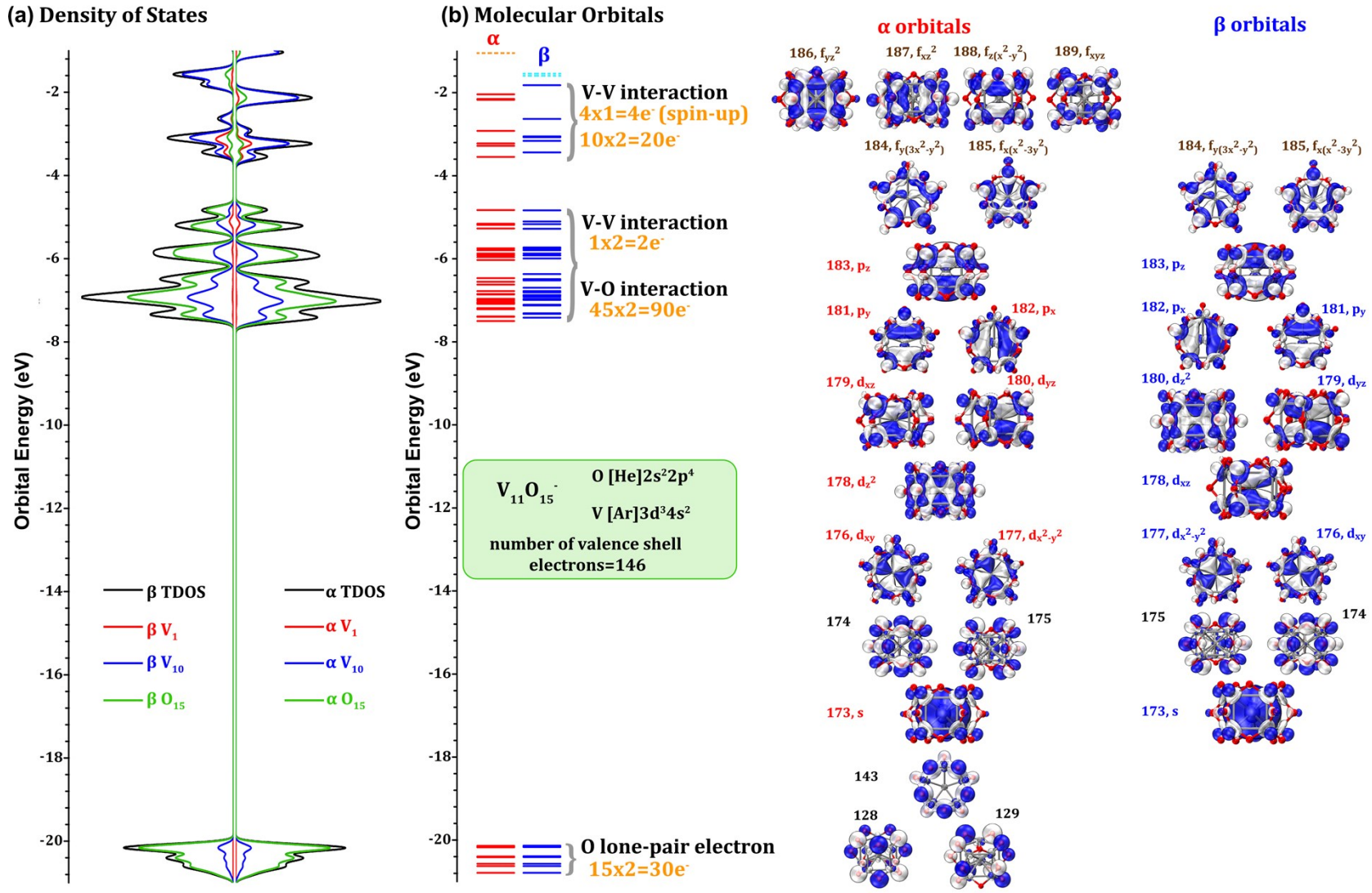

Fig. S13 (a) Total and partial density of states (DOS) and **(b)** canonical molecular orbitals (CMO) of the valence shell electrons of $V_{11}O_{15}^-$.

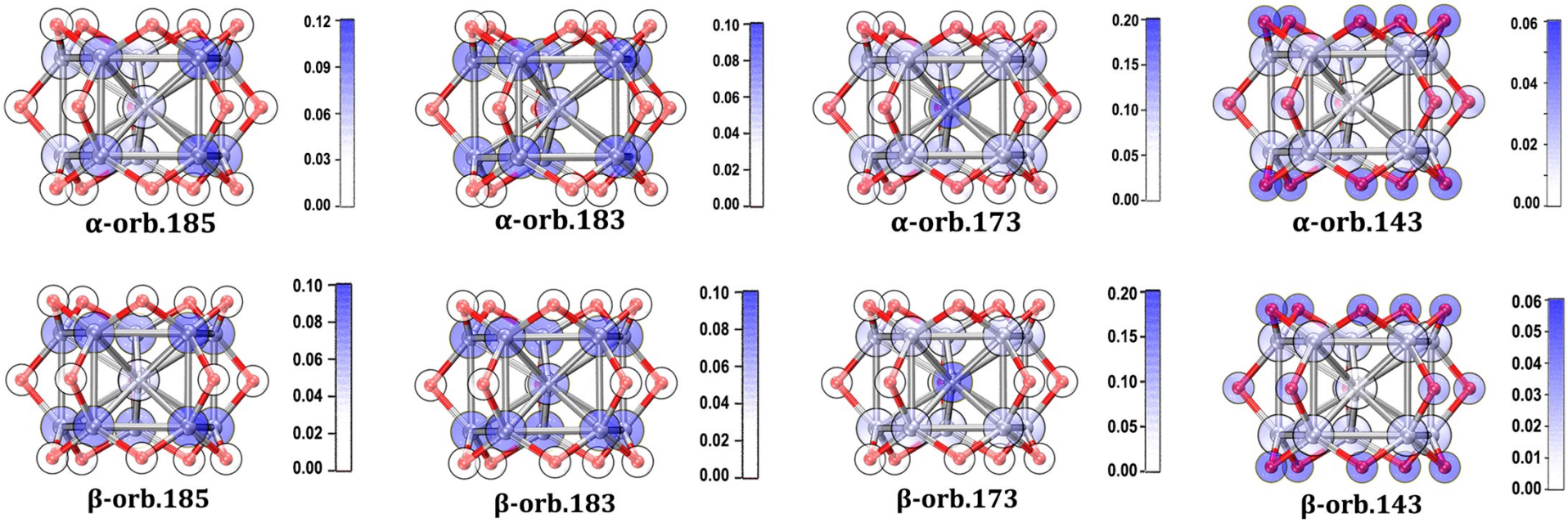

Fig. S14 Atomic orbital contributions to MO 185, 183, 173 and 143 based on natural atomic orbital (NAO) method. The composition numbers are listed in Table S5-S8.

3.8 A Comparison of $V_{11}O_{15}^-$ with $V_2O_5^-$

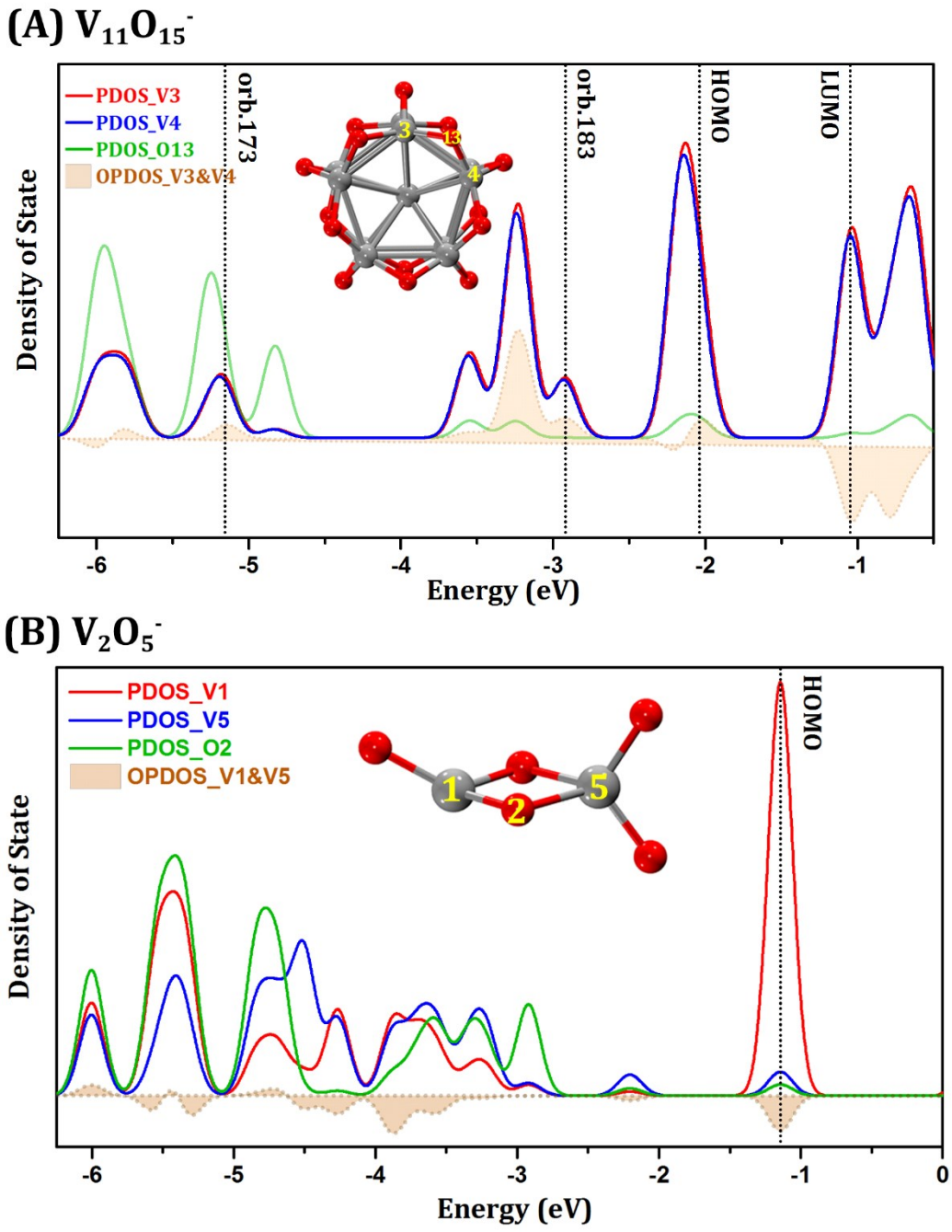

Fig. S15 The calculated partial density of states (PDOS) of the V-O-V unit in **(A)** $V_{11}O_{15}^-$ and **(B)** $V_2O_5^-$ at BP86/def2-TZVP level conducted by Multiwfn program[23] using SCPA method. The red line and blue line indicate the two vanadium atoms respectively and the green line indicates the oxygen atom between them. The brown area indicates the overlap population density of states (OPDOS) of the two vanadium atoms.

3.9 A Comparison with $V_{11}O_{15}^{+,0}$

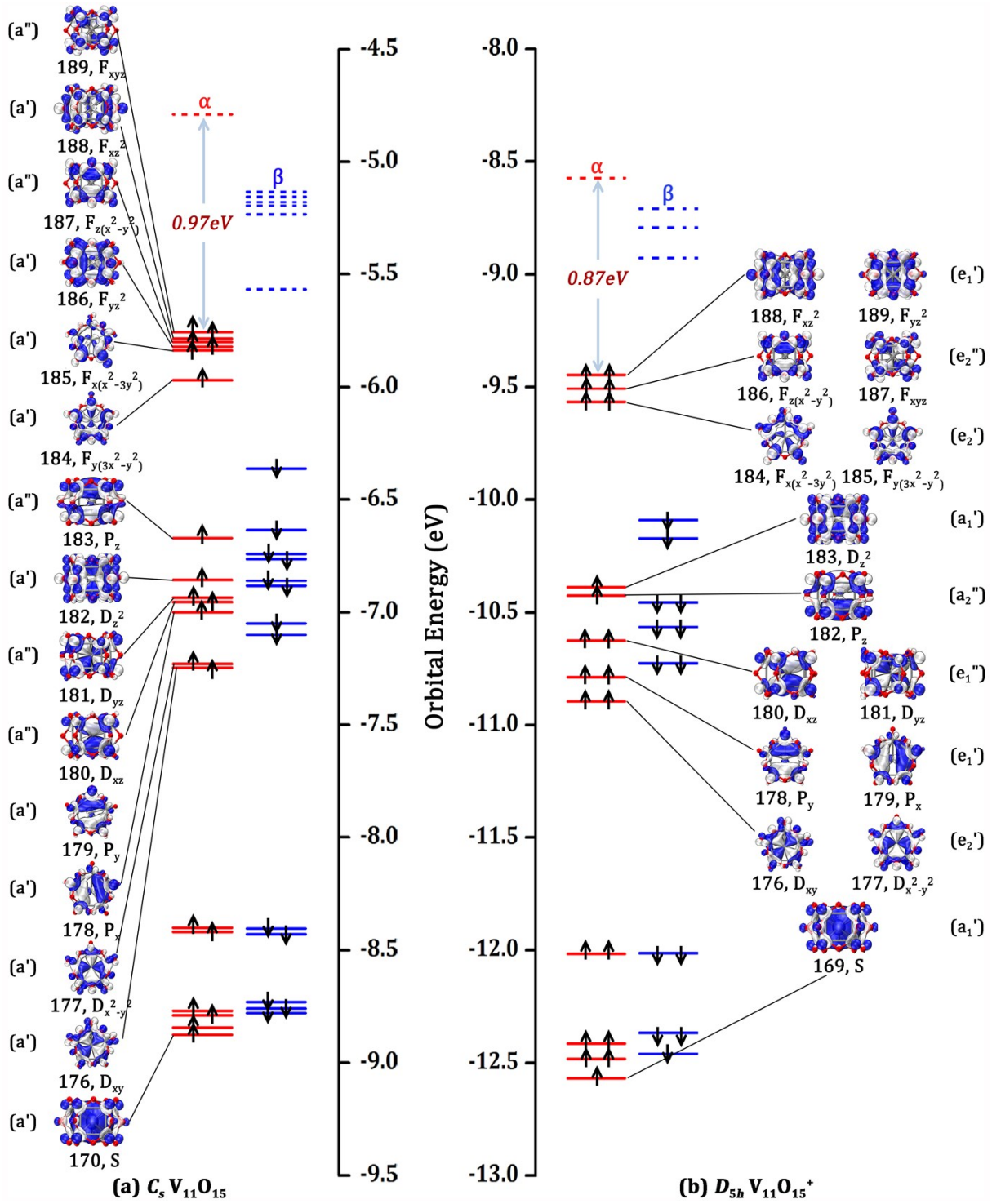

Fig. S16 The CMO energy levels of open-shell C_s $V_{11}O_{15}$ ($^6A'$) and D_{5h} $V_{11}O_{15}^+$ ($^7A_1'$) calculated at BP86/def2-TZVP level of theory, with the superatomic orbital features (S, P, D, and F) indicated.

3.10 NPA charge, electronic configuration, and bond order

Table S4 Natural atomic charges (q/|e|), electronic configurations, and Wiberg bond orders of the central V atom, the 10 V-ligands and 15 O-bridges in $V_{11}O_{15}^{\pm,0}$, calculated at BP86/def2-TZVP level of theory using NBO6.0 method.[16]

	Atoms	Atomic charges q	Electronic Configurations	Wiberg bond orders
D_{5h} $V_{11}O_{15}^-$ ($^5A_1'$)	V_1	−0.13	$[Ar]4s^{0.83}3d^{4.22}4p^{0.02}5S^{0.01}4d^{0.06}5d^{0.01}$	5.93
	$V_{2\text{-}11}$	+0.84	$[Ar]4s^{0.29}3d^{3.81}4p^{0.02}4d^{0.06}$	5.23
	$O_{1\text{-}10}$	−0.62	$[He]2s^{1.78}2p^{4.81}3s^{0.01}3p^{0.01}3d^{0.01}$	2.27
	$O_{11\text{-}15}$	−0.63	$[He]2s^{1.78}2p^{4.82}3p^{0.01}3d^{0.01}$	2.26
C_s $V_{11}O_{15}$ ($^6A'$)	V_1	−0.15	$[Ar]4s^{0.85}3d^{4.22}4p^{0.02}4d^{0.07}5d^{0.01}$	5.94
	$V_{2\text{-}11}$	+0.85 ~ +0.91	$[Ar]4s^{0.29}3d^{3.74\sim3.81}4p^{0.02}4d^{0.06}$	5.13~5.24
	$O_{1\text{-}15}$	−0.57 ~ −0.59	$[He]2s^{1.78\sim1.79}2p^{4.77\sim4.78}3s^{0\sim0.01}3p^{0.01}3d^{0.01}$	2.29~2.32
D_{5h} $V_{11}O_{15}^+$ ($^7A_1'$)	V_1	−0.17	$[Ar]4s^{0.87}3d^{4.21}4p^{0.02}5S^{0.01}4d^{0.08}5d^{0.01}$	5.92
	$V_{2\text{-}11}$	+0.93	$[Ar]4s^{0.28}3d^{3.73}4p^{0.02}4d^{0.06}$	5.12
	$O_{1\text{-}10}$	−0.54	$[He]2s^{1.78}2p^{4.74}3s^{0.01}3p^{0.01}3d^{0.01}$	2.36
	$O_{11\text{-}15}$	−0.55	$[He]2s^{1.78}2p^{4.74}3p^{0.01}3d^{0.01}$	2.34

3.11 Kohn-Sham orbital energy level correlation diagram in $V_{11}O_{15}^-$

The core-shell interaction between the interior mono-vanadium and the outer $V_{10}O_{15}$ cage can be also revealed by Kohn-Sham orbital energy-level correlation diagram between fragments based on the method of natural bond for chemical valence (NOCV)[39, 40]. Analysis of the energy decomposition analysis based on natural orbitals for chemical valence (EDA-NOCV), was conducted by using ADF software package. The BP86 functional combined with the all-electron Slater basis set of triple-zeta with polarization function (TZ2P) was employed. As indicated by the energy-level correlation diagram in Fig. S18, the superatomic S orbital of D_{5h} $V_{11}O_{15}^-$ is contributed by both the $4s^2$ orbital of V^- and the correlated orbital of $V_{10}O_{15}$ moiety. Similarly, the superatomic D orbital of D_{5h} $V_{11}O_{15}^-$ is also contributed by the both fragments. In comparison, the superatomic P and F orbitals are mainly contributed by the outer $V_{10}O_{15}$ fragment (actually mainly by V_{10} as revealed in Fig. 3 of the main text) which functions as a shield for *d-d* and *s-s* coordination allowing correlative electrons to occupy the lower energy levels, hence enhanced stability of the D_{5h} $V_{11}O_{15}^-$ cluster.

Fig. S17 provides a comparison with the canonical molecular orbital (CMO) energy levels of D_{5h} $V_{11}O_{15}^{+}$ ($^{7}A_{1}'$) and C_{s} $V_{11}O_{15}$ ($^{6}A_{1}$). Interestingly, both exhibit obvious open-shell superatomic orbital features, but the former cation exhibits more degenerate orbitals than the latter neutral. The D_{5h} $V_{11}O_{15}^{+}$ ($^{7}A_{1}'$) has an electronic configuration of $S^{2}P^{6}D^{10}F^{6}$ possessing six spin-up unpaired electrons, allowing the addition of one or two more electrons in C_{s} $V_{11}O_{15}$ ($^{6}A_{1}$) and D_{5h} $V_{11}O_{15}^{-}$ ($^{5}A_{1}'$) to fill the beta orbitals. Although the three clusters $V_{11}O_{15}^{\pm,0}$ have a similar geometric structure, the relatively lower symmetry and higher spin multicity of $V_{11}O_{15}^{+,0}$ account for their lower stability, which is in consistent with the mass spectrometry observations.

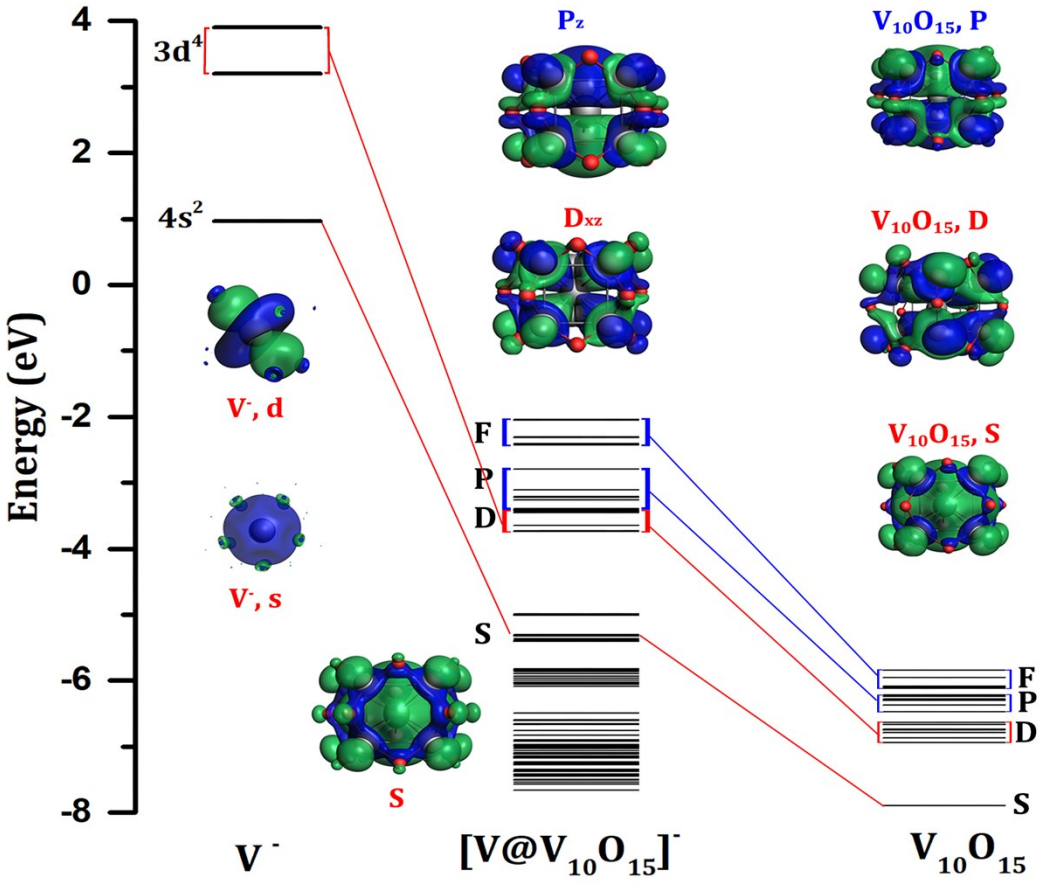

Fig. S17 Kohn-Sham energy-level correlation diagram of D_{5h} $V_{11}O_{15}^{-}$ cluster. Inset: The proposed superatom-atom orbital modellings.

3.12 Atomic orbital contribution

Table S5 Atomic orbital contribution to α-MO.183 based on NAO method.

Center	Composition
1(V)	6.24%
2(V)	8.89%
3(V)	8.89%
4(V)	8.89%
5(V)	8.89%
6(V)	8.89%
7(V)	8.89%
8(V)	8.89%
9(V)	8.89%
10(V)	8.89%
11(V)	8.89%
12(O)	0.02%
13(O)	0.02%
14(O)	0.02%
15(O)	0.02%
16(O)	0.02%
17(O)	0.02%
18(O)	0.02%
19(O)	0.02%
20(O)	0.02%
21(O)	0.02%
22(O)	0.81%
23(O)	0.81%
24(O)	0.81%
25(O)	0.81%
26(O)	0.81%

Table S6 Orbital composition analysis of α-MO.183 based on NAO method.

NAO#	Center	Label	Type	Composition
17	1(V)	pz	Val(4p)	4.83%
166	4(V)	dx2y2	Val(3d)	3.27%
346	8(V)	dx2y2	Val(3d)	3.27%
64	2(V)	dxy	Val(3d)	2.96%
244	6(V)	dxy	Val(3d)	2.96%
424	10(V)	dxy	Val(3d)	2.96%
469	11(V)	dxy	Val(3d)	2.96%
80	2(V)	dz2	Val(3d)	2.76%
125	3(V)	dz2	Val(3d)	2.76%
170	4(V)	dz2	Val(3d)	2.76%
215	5(V)	dz2	Val(3d)	2.76%
260	6(V)	dz2	Val(3d)	2.76%
305	7(V)	dz2	Val(3d)	2.76%
350	8(V)	dz2	Val(3d)	2.76%
395	9(V)	dz2	Val(3d)	2.76%
440	10(V)	dz2	Val(3d)	2.76%
485	11(V)	dz2	Val(3d)	2.76%
121	3(V)	dx2y2	Val(3d)	2.14%
211	5(V)	dx2y2	Val(3d)	2.14%
301	7(V)	dx2y2	Val(3d)	2.14%
391	9(V)	dx2y2	Val(3d)	2.14%
16	1(V)	pz	Cor(3p)	1.42%
109	3(V)	dxy	Val(3d)	1.13%
199	5(V)	dxy	Val(3d)	1.13%
289	7(V)	dxy	Val(3d)	1.13%
379	9(V)	dxy	Val(3d)	1.13%
148	4(V)	py	Val(4p)	1.06%
328	8(V)	py	Val(4p)	1.06%
……	…	……	……	……
			Summing up the compositions listed above:	99.43%
			Rydberg composition:	0.57%

Note: Cor: core NAO; Val: valence shell NAO.

Table S7 Atomic orbital contribution to α-MO.173 based on NAO method.

Center	Composition
1(V)	19.48%
2(V)	7.86%
3(V)	7.86%
4(V)	7.86%
5(V)	7.86%
6(V)	7.86%
7(V)	7.86%
8(V)	7.86%
9(V)	7.86%
10(V)	7.86%
11(V)	7.86%
12(O)	0.07%
13(O)	0.07%
14(O)	0.07%
15(O)	0.07%
16(O)	0.07%
17(O)	0.07%
18(O)	0.07%
19(O)	0.07%
20(O)	0.07%
21(O)	0.07%
22(O)	0.22%
23(O)	0.22%
24(O)	0.21%
25(O)	0.21%
26(O)	0.22%

Table S8 Orbital composition analysis of α-MO.173 based on NAO method.

NAO#	Center	Label	Type	Composition
4	1(V)	S	Val(4S)	13.10%
3	1(V)	S	Cor(3S)	6.00%
162	4(V)	dyz	Val(3d)	2.84%
342	8(V)	dyz	Val(3d)	2.84%
113	3(V)	dxz	Val(3d)	2.57%
203	5(V)	dxz	Val(3d)	2.57%
293	7(V)	dxz	Val(3d)	2.57%
383	9(V)	dxz	Val(3d)	2.57%
49	2(V)	S	Val(4S)	1.93%
94	3(V)	S	Val(4S)	1.93%
139	4(V)	S	Val(4S)	1.93%
184	5(V)	S	Val(4S)	1.93%
229	6(V)	S	Val(4S)	1.93%
274	7(V)	S	Val(4S)	1.93%
319	8(V)	S	Val(4S)	1.93%
364	9(V)	S	Val(4S)	1.93%
409	10(V)	S	Val(4S)	1.93%
454	11(V)	S	Val(4S)	1.93%
72	2(V)	dyz	Val(3d)	1.86%
252	6(V)	dyz	Val(3d)	1.86%
432	10(V)	dyz	Val(3d)	1.86%
477	11(V)	dyz	Val(3d)	1.86%
166	4(V)	dx2y2	Val(3d)	1.57%
346	8(V)	dx2y2	Val(3d)	1.57%
64	2(V)	dxy	Val(3d)	1.42%
244	6(V)	dxy	Val(3d)	1.42%
424	10(V)	dxy	Val(3d)	1.42%
469	11(V)	dxy	Val(3d)	1.42%
121	3(V)	dx2y2	Val(3d)	1.03%
211	5(V)	dx2y2	Val(3d)	1.03%
301	7(V)	dx2y2	Val(3d)	1.03%
391	9(V)	dx2y2	Val(3d)	1.03%
……	……	……	……	……
			Summing up the compositions listed above:	99.80%
			Rydberg composition:	0.20%

Note: Cor: core NAO; Val: valence shell NAO.

S4. References

1. H. Zhang, H. Wu, Y. Jia, L. Geng, Z. Luo, H. Fu and J. Yao, *Rev. Sci. Instrum.*, 2019, **90**, 073101.
2. H. Zhang, H. Wu, L. Geng, Y. Jia, M. Yang and Z. Luo, *Phys. Chem. Chem. Phys.*, 2019, **21**, 11234-11241.
3. A. Armstrong, H. Zhang, A. C. Reber, Y. Jia, H. Wu, Z. Luo and S. N. Khanna, *J. Phys. Chem. A*, 2019, **123**, 7463-7469.
4. H. Zhang, A. C. Reber, L. Geng, D. Rabayda, H. Wu, Z. Luo, J. Yao and S. N. Khanna, *CCS Chemistry*, 2019, 571-581.
5. J. Wang, D. Hao, J. Ye and N. Umezawa, *Chem. Mater.*, 2017, **29**, 2694-2707.
6. G. Kresse and J. Furthmüller, *Phys. Rev. B*, 1996, **54**, 11169-11186.
7. Y. Zhao, X. Chen and J. Li, *Nano Research*, 2017, **10**, 3407-3420.
8. J. P. Perdew, K. Burke and M. Ernzerhof, *Phys. Rev. Lett.*, 1996, **77**, 3865-3868.
9. J. P. Perdew and Y. Wang, *Phys. Rev. B*, 1992, **45**, 13244-13249.
10. J. P. Perdew, *Phys. Rev. B*, 1986, **33**, 8822-8824.
11. A. D. Becke, *Phys. Rev. A*, 1988, **38**, 3098-3100.
12. A. Schäfer, C. Huber and R. Ahlrichs, *J. Chem. Phys.*, 1994, **100**, 5829-5835.
13. M. J. Frisch, G. W. Trucks, H. B. Schlegel, G. E. Scuseria, M. A. Robb, J. R. Cheeseman, G. Scalmani, V. Barone, B. Mennucci, G. A. Petersson, H. Nakatsuji, M. Caricato, X. Li, H. P. Hratchian, A. F. Izmaylov, J. Bloino, G. Zheng, J. L. Sonnenberg, M. Hada, M. Ehara, K. Toyota, R. Fukuda, J. Hasegawa, M. Ishida, T. Nakajima, Y. Honda, O. Kitao, H. Nakai, T. Vreven, J. A. Montgomery, J. E. Peralta, F. Ogliaro, M. Bearpark, J. J. Heyd, E. Brothers, K. N. Kudin, V. N. Staroverov, R. Kobayashi, J. Normand, K. Raghavachari, A. Rendell, J. C. Burant, S. S. Iyengar, J. Tomasi, M. Cossi, N. Rega, J. M. Millam, M. Klene, J. E. Knox, J. B. Cross, V. Bakken, C. Adamo, J. Jaramillo, R. Gomperts, R. E. Stratmann, O. Yazyev, A. J. Austin, R. Cammi, C. Pomelli, J. W. Ochterski, R. L. Martin, K. Morokuma, V. G. Zakrzewski, G. A. Voth, P. Salvador, J. J. Dannenberg, S. Dapprich, A. D. Daniels, Farkas, J. B. Foresman, J. V. Ortiz, J. Cioslowski and D. J. Fox, Gaussian 09 Rev. E.01.
14. K. P. Jensen, B. O. Roos and U. Ryde, *J. Chem. Phys.*, 2007, **126**, 014103.
15. J. VandeVondele, M. Krack, F. Mohamed, M. Parrinello, T. Chassaing and J. Hutter, *Comput. Phys. Commun.*, 2005, **167**, 103-128.
16. E. D. Glendening, C. R. Landis and F. Weinhold, *J. Comput. Chem.*, 2013, **34**, 1429-1437.
17. D. Y. Zubarev and A. I. Boldyrev, *Phys. Chem. Chem. Phys.*, 2008, **10**, 5207-5217.
18. H. X. Shi, W. G. Sun, X. Y. Kuang, C. Lu, X. X. Xia, B. L. Chen and A. Hermann, *J. Phys. Chem. C*, 2017, **121**, 24886-24893.
19. S. Klod and E. Kleinpeter, *J. Chem. Soc., Perkin Trans. 2*, 2001, 1893-1898.
20. E. Kleinpeter, S. Klod and A. Koch, *J. Mol. Struct.: THEOCHEM*, 2007, **811**, 45-60.
21. K. Wolinski, J. F. Hinton and P. Pulay, *J. Am. Chem. Soc.*, 1990, **112**, 8251-8260.
22. R. Ditchfield, *Mol. Phys.*, 1974, **27**, 789-807.
23. Tian Lu and F. Chen, *J. Comput. Chem.*, 2012, **33**, 580-592.
24. W. Humphrey, A. Dalke and K. Schulten, *J. Mol. Graph.*, 1996, **14**, 33-38.
25. A. D. Becke, *J. Chem. Phys.*, 1993, **98**, 5648-5652.
26. C. T. Lee, W. T. Yang and R. G. Parr, *Phys. Rev. B*, 1988, **37**, 785-789.
27. K. R. Asmis and J. Sauer, *Mass Spectrom. Rev.*, 2007, **26**, 542-562.
28. S. F. Vyboishchikov and J. Sauer, *J. Phys. Chem. A*, 2000, **104**, 10913-10922.
29. B. Xu, Y.-X. Zhao, X.-L. Ding, Q.-Y. Liu and S.-G. He, *J. Phys. Chem. A*, 2013, **117**, 2961-2970.
30. E. Jakubikova, A. K. Rappe and E. R. Bernstein, *J. Phys. Chem. A*, 2007, **111**, 12938-12943.
31. R. Jin, C. Zeng, M. Zhou and Y. Chen, *Chem. Rev. (Washington, DC, U. S.)*, 2016, **116**, 10346-10413.

32. J. Yan, H. Su, H. Yang, S. Malola, S. Lin, H. Haekkinen and N. Zheng, *J. Am. Chem. Soc.*, 2015, **137**, 11880-11883.
33. J. F. Parker, C. A. Fields-Zinna and R. W. Murray, *Acc. Chem. Res.*, 2010, **43**, 1289-1296.
34. Y. Yu, Z. Luo, D. M. Chevrier, D. T. Leong, P. Zhang, D.-e. Jiang and J. Xie, *J. Am. Chem. Soc.*, 2014, **136**, 1246-1249.
35. O. Lopez-Acevedo, H. Tsunoyama, a. Tsukuda, H. Hakkinen and C. M. Aikens, *J. Am. Chem. Soc.*, 2010, **132**, 8210–8218.
36. O. Fuhr, S. Dehnen and D. Fenske, *Chem. Soc. Rev.*, 2013, **42**, 1871-1906.
37. X. Kang and M. Zhu, *Chem. Soc. Rev.*, 2019, **48**, 2422-2457.
38. S. Takano, S. Ito and T. Tsukuda, *J. Am. Chem. Soc.*, 2019, **141**, 15994-16002.
39. A. Michalak, M. Mitoraj and T. Ziegler, *J. Phys. Chem. A*, 2008, **112**, 1933-1939.
40. M. Mitoraj and A. Michalak, *J. mol. model.*, 2007, **13**, 347-355.